



## RESEARCH ARTICLE

# Extreme Greenland blocking and high-latitude moisture transport

Bradford S. Barrett<sup>1</sup> | Gina R. Henderson<sup>1</sup> | Erin McDonnell<sup>1</sup> |  
Major Henry<sup>1</sup> | Thomas Mote<sup>2</sup>

<sup>1</sup>Oceanography Department, U.S. Naval Academy, Annapolis, Maryland

<sup>2</sup>Geography Department, University of Georgia, Athens, Georgia

**Correspondence**

Bradford S. Barrett, Oceanography Department, U.S. Naval Academy, 572C Holloway Rd, Annapolis, MD 21402.  
Email: bbarrett@usna.edu

**Funding information**

Strategic Environmental Research and Development Program (SERDP), Grant/Award Number: RC18-1658

**Abstract**

Blocked atmospheric flows over Greenland and the North Atlantic Arctic (NAA) can be defined by the appearance of an anomalous ridge, many times off the western margin of continents, that deflects traveling cyclones from their usual storm tracks. Atmospheric blocking often produces a strong equatorward deflection of polar air on the eastern flank of the anticyclone, including severe cold episodes in winter, and severe droughts and heat waves in summer. Recent changes in low-frequency atmospheric circulation in the NAA have increased sensible heat and moisture advection from the mid-latitudes into this region. In this study, we explore the frequency and seasonality of extreme Greenland blocking, and we explore the relationship between extreme blocking and moisture transport into and over the region.

We quantify atmospheric flow blocking over Greenland using the Greenland Blocking Index, and extreme blocking is defined from 1980 to 2019 at the 90th, 95th, 97th, and 99th percentiles for both summer (June to August) and winter (December to February) seasons. Moisture transport over Greenland was defined by calculating daily integrated vapor transport from the ERA-Interim reanalysis over the region from 15° to 85°W and 55° to 80°N. The frequency of extreme blocking over Greenland was found to have increased in the most recent two decades (2000–2019) compared to the period 1980–1999. In addition, the probability of above-average moisture transport occurring on a day with extreme blocking is high in both summer and winter, with the highest probability of high moisture transport during an extreme Greenland Blocking Index day in winter. These findings are unique to this work and suggest future work on the role of moisture transport in developing or sustaining blocks over Greenland.

**KEYWORDS**

extreme Greenland blocking, integrated vapor transport

This is an open access article under the terms of the Creative Commons Attribution License, which permits use, distribution and reproduction in any medium, provided the original work is properly cited.

© 2020 The Authors. *Atmospheric Science Letters* published by John Wiley & Sons Ltd on behalf of the Royal Meteorological Society.

## 1 | INTRODUCTION

Atmospheric flow blocking can be defined by the appearance of an anomalous center of high pressure or mid-tropospheric ridge, many times off the western margin of continents, that deflects traveling cyclones from their usual storm tracks (Rex, 1950a,b; Namias, 1982; Rasmusen and Wallace, 1983; Legras and Ghil, 1985). This anticyclone is often associated with a breakdown of the high kinetic energy state of the atmosphere into a low kinetic energy state, possibly even reversing mid-latitude westerly flow to easterly (Tibaldi and Molteni, 1990; Scherrer *et al.*, 2006; Tyrllis and Hoskins, 2008). Atmospheric blocking can cause a strong equatorward deflection of polar air on the eastern flank of the anticyclone, leading to severe cold episodes in winter (Dole and Gordon, 1983; Hoskins and Sardeshmukh, 1987) and severe droughts and heat waves in summer (Black *et al.*, 2004; Dole *et al.*, 2011). Over Greenland, flow blocking results in a large-scale reversal of the meridional geopotential height gradient, a potential increase in surface temperature (Pelly and Hoskins, 2003), and possible changes in ice mass balance (McLeod and Mote, 2016). The occurrence of flow blocking is thus of critical interest to both weather and climate.

Many metrics have been created to identify and quantify atmospheric flow blocking. Some involve hierarchical methods (spatial clustering; Cheng and Wallace, 1993) and non-hierarchical (partitioning) methods (Michelangeli *et al.*, 1995), while others use mixture model (Smyth *et al.*, 1999) and nonlinear equilibrium methods (Vautard, 1990). Still other techniques involve measures of the strength of the westerly flow (Lejenas and Okland, 1983; Tibaldi and Molteni, 1990; Pelly and Hoskins, 2003) and of persistent height anomalies (Dole and Gordon 1983; Dole 1986). Recently, a Greenland Blocking Index (GBI) has been defined by Fang (2004) to examine atmospheric flow blocking over and around Greenland. The GBI has found many uses (Hanna *et al.*, 2013; 2014; 2015), perhaps owing to its ability to clearly and simply depict blocking—and changes in blocking—across the Greenland region. The GBI is strongly correlated with other similar blocking indices, including those of Davini *et al.* (2012) and Scherrer *et al.* (2006), and it is useful in detecting not only long-term but also instantaneous blocking (Davini *et al.*, 2012; 2013), changes in regional blocking features (Overland *et al.*, 2015), changes in ice surface mass balance (Hanna *et al.* 2013; McCloud and Mote, 2016) and Arctic amplification (Francis and Vavrus, 2015).

Because the GBI captures geopotential height over a relatively large sector of the North Atlantic Arctic, it is also linked to other major modes of atmospheric

variability in the region. For example, decreases in the North Atlantic Oscillation (NAO; Hurrell *et al.*, 2003) index in summer have been related to an increasing trend in GBI in summer, while record high and low NAO values in early winter (December) have contributed to variability in the GBI (Hanna *et al.*, 2014). Rossby wave breaking is known to be related to the NAO, and thus high-latitude circulation around Greenland. A positive NAO (low heights over Greenland) was related to unblocked flow by Woollings *et al.* (2008), while a negative NAO (high heights over Greenland) was related to blocked flows and above-normal heights over Greenland (Rennert and Wallace, 2009). A similar pattern, but in temperature anomalies, has been found between Greenland blocking and the NAO, whereby during blocked flows a “low-high-low” pattern in temperatures develops over North America, Greenland, and Northern Europe, respectively (Masato *et al.*, 2012; Croci-Maspoli *et al.*, 2007). On longer time scales, the Pacific Decadal Oscillation (PDO; Mantua *et al.*, 1997) influences geopotential heights over a broad swath of the high latitudes in the Northern Hemisphere. In winter, the PDO's relationship to geopotential height at 500 hPa is primarily via a wave train over the central Pacific Ocean extending north of Alaska, while in the summer, the wave train extends from the western Pacific across the Arctic, to Greenland (where the correlation between PDO and 500 hPa height is negative) and then to Europe (Collow *et al.*, 2017). In this study, we use the GBI to quantify both variability in extreme atmospheric flow blocking over Greenland and relationships between extreme blocking and moisture transport.

Moisture and moisture transport in the Arctic have received renewed attention recently, partly because of strong warming in surface temperatures in this region, significantly above worldwide trends (Polyakov *et al.*, 2002; Serreze *et al.*, 2009; Screen and Simmonds, 2010; Hartmann *et al.*, 2013). The northern North Atlantic stands out as a main gateway for moisture transport to the Arctic, and that channel is linked strongly to transient eddies in the mean circulation, particularly for southwest Greenland (Dufour *et al.*, 2016). Overall, the Arctic atmosphere north of 70°N has been steadily moistening (Held and Soden, 2006; Gimeno *et al.*, 2014; Lavers *et al.*, 2015; Rinke *et al.*, 2019). Over Greenland, “moist” days (defined as days with anomalously high water vapor transport to Greenland) have increased in frequency between 1979 and 2015 (Mattingly *et al.*, 2016). Summer moisture transport over Greenland has tended to receive the most attention in the literature (Yang and Magnusdottir, 2017; Mattingly *et al.*, 2018), due to its link to surface ice mass balance, but transient eddy fluxes over the Greenland Sea (east of Greenland) are comparable for both winter and summer

(Dufour *et al.*, 2016). Indeed, the relative fraction of moisture transport to the Arctic from the Atlantic has been found to be greatest from October through March (Gimeno-Sotelo *et al.*, 2018), and traveling cyclone activity over and east of Greenland (whose paths and intensities are impacted by Greenland flow blocking; McCloud and Mote, 2015) is responsible for more than half of moisture transport into the Arctic (Sorteberg and Walsh, 2008). Rossby wave breaking and blocking has been linked to moisture transport in the Arctic (Woods *et al.*, 2013), including more distant moisture sources during periods of high Greenland blocking (Nusbaumer *et al.*, 2019), and southwest Greenland has emerged as perhaps a favored channel and impact zone for that transport (Liu and Barnes, 2015). What has been studied in relatively less detail (e.g., Nygård *et al.*, 2019), and what thus motivated this current study, is the trends in *extreme Greenland* blocking and the links between *extreme* blocking and moisture transport over Greenland. The remainder of this article is organized as follows: data and methods are described in Section 2, results are presented in Section 3, and conclusions are presented in Section 4.

## 2 | DATA AND METHODS

The analyses in this study were based on two publicly available data sets. First, Greenland blocking was quantified using the daily GBI (Hanna *et al.*, 2013) over the 40-year period January 1980 to December 2019. The GBI is the mean 500-hPa geopotential height over the Greenland region, from 20° to 80°W and 60° to 80°N (Figure 1),

and the daily index is available from <https://www.esrl.noaa.gov/psd/data/timeseries/daily/GBI/>. In this study, a “block” is referring to an instantaneous block, including transient high-pressure systems and persistent blocking events, and does not distinguish between the two. *Extreme* blocking was calculated for summer (June to August; JJA) and winter (December to February; DJF) by identifying the daily GBI values that correspond to four thresholds of extremity: the 90th, 95th, 97th, and 99th percentiles. Percentile values for each threshold were calculated separately for each season by first sorting the daily data and then linearly interpolating to compute percentiles for percentages between  $100(0.5/n)$  and  $100([n - 0.5]/n)$ , where  $n$  is the number of elements in the dataset (Langford, 2006). Physically, an extreme positive GBI indicates highly anomalous instantaneous ridging over Greenland (McCloud and Mote, 2015), and in this case, the mean height field during the 95th percentile featured instantaneous ridging centered over southeast Greenland in winter (DJF) and south-central Greenland in summer (JJA) (Figure 1). The height values corresponding to the 90th, 95th, 97th, and 99th percentiles in DJF are 5,280.6, 5,333.8, 5,368.2, and 5,439.0 m, respectively, and in JJA are 5,593.3, 5,618.5, 5,636.4, and 5,658.2 m (Table 1). Second, moisture transport over Greenland was quantified using integrated vapor transport (IVT), which was calculated from the ERA-interim reanalysis (Dee *et al.*, 2011), following the methodology of Rutz *et al.* (2014) and Mattingly *et al.* (2016):

$$IVT = \frac{1}{g} \int_{1,000\text{hPa}}^{200\text{hPa}} qVdp, \tag{1}$$

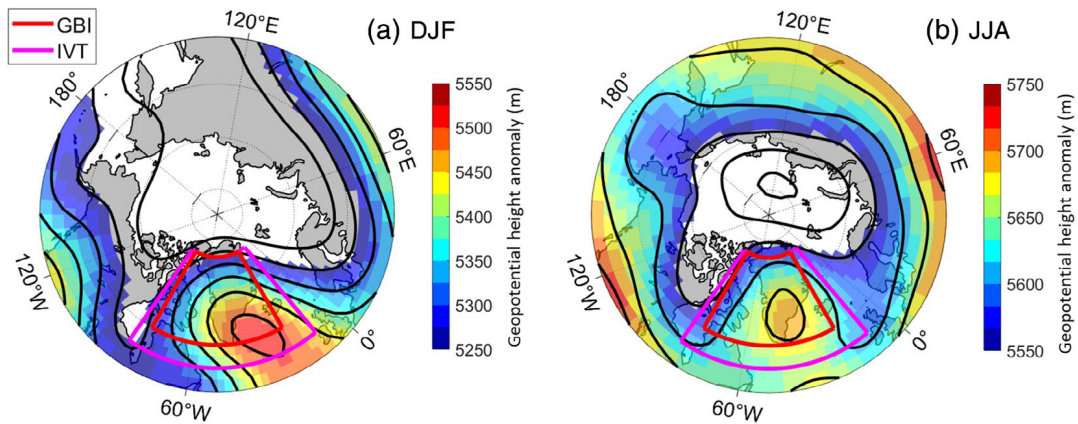


**FIGURE 1** Height field (in m) at 500-hPa on days in (a) DJF and (b) JJA when the NOAA Greenland Blocking Index (GBI) was above the 95th percentile. Both shading and contours indicate mean heights, and contours are drawn between 5,200 and 5,800 m at 60-m increments. Red boxed region indicates the spatial domain averaged to calculate the NOAA GBI index, and the magenta boxed region indicates the domain used to calculate integrated vapor transport (IVT) from the ERA-interim reanalysis. Note the color scale is different in panel (a) and (b)

**TABLE 1** Frequencies of extreme GBI events (days with GBI index in the 90th, 95th, 97th, or 99th percentiles) by year: 1980–1999 and 2000–2019, for winter (DJF) and summer (JJA) months, calculated for the period including 2010 (an extreme NAO year) and excluding 2010

Percentile of GBI values	Including 2010				Excluding 2010				
	Season	Total occurrences within GBI	Threshold height (m)	Percent of Occurrences		Total occurrences within GBI	Threshold height (m)	Percent of occurrences	
				1980–1999	2000–2019			1980–1999	2000–2019
90th	DJF	358	5280.6	41.9%	58.1%	305	5271.2	49.2%	50.8%
	JJA	368	5593.3	28.0%	72.0%	352	5592.6	29.3%	70.7%
95th	DJF	179	5333.8	38.0%	62.0%	142	5322.0	47.9%	52.1%
	JJA	184	5618.5	25.5%	74.5%	178	5618.4	26.4%	73.6%
97th	DJF	107	5368.2	30.8%	69.2%	80	5349.9	41.3%	58.8%
	JJA	110	5636.4	23.6%	76.4%	105	5635.8	24.8%	75.2%
99th	DJF	36	5439.0	19.4%	80.6%	26	5423.0	26.9%	73.1%
	JJA	37	5658.2	16.2%	83.8%	34	5657.5	17.6%	82.4%

where  $q$  and  $V$  are the specific humidity (in  $\text{kg}\cdot\text{kg}^{-1}$ ) and wind vector (in  $\text{m}\cdot\text{s}^{-1}$ ) at pressure level  $p$ ,  $dp$  is the difference between consecutive pressure levels (50-hPa intervals between 1,000 and 500 hPa and 100-hPa intervals between 500 and 200 hPa), and  $g$  is the gravitational acceleration ( $9.80655 \text{ m}\cdot\text{s}^{-2}$ ). Daily IVT values were calculated at 1200 UTC each day from January 1980 to August 2019 at each grid point in the ERA-interim reanalysis. To examine moisture transport around Greenland specifically, IVT was spatially averaged over the region from  $15^\circ$  to  $85^\circ\text{W}$  and  $55^\circ$  to  $80^\circ\text{N}$  (Figure 1). Finally, similar to GBI, extreme thresholds of IVT around Greenland were calculated at the 90th, 95th, 97th, and 99th percentiles for both DJF and JJA.

### 3 | RESULTS

#### 3.1 | Changes in Greenland blocking over time

The first part of this study explored whether occurrences of extreme Greenland blocking have changed over the 40-year period. In winter (DJF) 1980–2019, there were 358 occurrences of blocking at the 90th percentile, and only 150 (or 41.9%) of them occurred from 1980 to 1999 (Table 1). As the extremity of Greenland blocking increased, this disparity increased: only 38.0% of the 95th percentile blocking events occurred in the first half of the period, and only 30.8% and 19.4% of the 97th and 99th percentile events occurred in the first half of the period. This means that extreme winter Greenland blocking has become more common in the recent two decades, and particularly so for the most extreme (the 99th percentile) blocking days, when compared to the previous two decades. In summer, the trends in extreme Greenland blocking frequency between 1980 and 2019 are even more pronounced, and not confined to the most extreme percentiles. For example, 72.0% of the 90th percentile days occurred from 2000 to 2019, and 74.5% of the 95th, 76.4% of the 97th, and 83.8% of the 99th percentile days occurred in the most recent two decades (Table 1). It is important to note that work by Collow *et al.* (2017) found negative correlations between the PDO and 500-hPa heights over Greenland in summer (but not winter), so some of the signal we show here in GBI may be due to decadal variability associated with other elements of the climate system. That is suggested as an area of future work.

Because DJF 2009–2010 was a winter with extreme NAO values (NAO index of  $-2.4$ ; Osborn, 2011), the frequency of extreme blocking from 2000 to 2019 was re-computed for each percentile omitting 2010. Because

there is one fewer year in the period, the expected frequencies drop to 52% in 1980–1999 and 48% in the latter period. As noted in Table 1, the frequency of extreme winter GBI above the 90th, 95th, and 97th percentiles reduce to 50.8%, 52.1%, and 58.8% respectively, when 2010 is excluded, but the frequency of GBI above the 99th percentile remains high (at 73.1%). The frequency of extreme GBI in summer remained largely unchanged when 2010 was excluded. This result suggests that variability in extreme NAO can impact the frequency of extreme Greenland blocking in winter, in agreement with Woollings *et al.* (2008) and Rennert and Wallace (2009).

Patterns in frequency of extreme Greenland blocking are also seen in a time series of yearly occurrences (Figure 2). There, the interannual variability in extremes is evident. In winter, extremes tend to cluster in multi-year groupings, including 2009–2011. Moreover, some years, notably 1991–1993 and 2012–2015, had no extremes above the 90th percentile (Figure 2a). This interannual clustering agrees with Ding *et al.* (2014) and Li *et al.* (2019) who noted that interannual variability in blocking can be linked to the El Niño-Southern Oscillation. In summer, the increase in frequency of extreme blocking is evident, with no years with more than 15 extreme days (above the 90th percentile) prior to 1995, but two out of every 3 years after 2005 with more than 15 extreme events above the 90th percentile (Figure 2b). In both seasons, the increase in the frequency of the most extreme (97th and 99th) blocking is evident, and the clustering of extreme blocking from 2005 to 2011 is

particularly notable. The changes in extreme blocking are reflected in shifts in the distributions of the GBI index in both winter (Figure 3a) and summer (Figure 3(b)). From 1980 to 2019, the distributions appear to shift right, with the extremes in the right tail shifting right as well. For example, in winter, the 90th, 95th, 97th, and 99th percentile values from 1980 to 1999 correspond to the 86.1th, 93.1th, 94.9th, and 96.6th percentiles in 2000–2019. Put another way, the 99th percentile winter GBI value in the first half of the record was 5,388.3 m; in the second half of the record, the 99th percentile was 5,464.9 m, an increase of 76.6 m. In summer, the 90th percentile GBI from 1980–1999 became the 76.5th percentile from 2000 to 2019; the 95th, 97th, and 99th percentile GBI values became the 87.4th, 91.6th, and 96.5th. Moreover, for both the DJF and JJA seasons, the 1980–1999 and 2000–2019 distributions are statistically significantly different using the one-sample Kolmogorov–Smirnov test (Massey, 1951; Miller, 1956; Marsaglia *et al.*, 2003), with *p*-values less than 0.01 indicating significance beyond the 99% confidence level. These shifts in extremes confirm that the magnitudes of extreme blocking, as captured by the GBI index, are changing over this time period, and that blocking events that were once extreme (in the first part of the period, 1980–1999) are becoming more common. This trend in extreme blocking from 1980–2019 mirrors some of the longer-term trends, whereby periods of sustained high GBI in the late 1800s (1870–1900) were similar to the more current trends (2000–2019) (Hanna *et al.*, 2018). However, the clustering of extreme high GBI events since

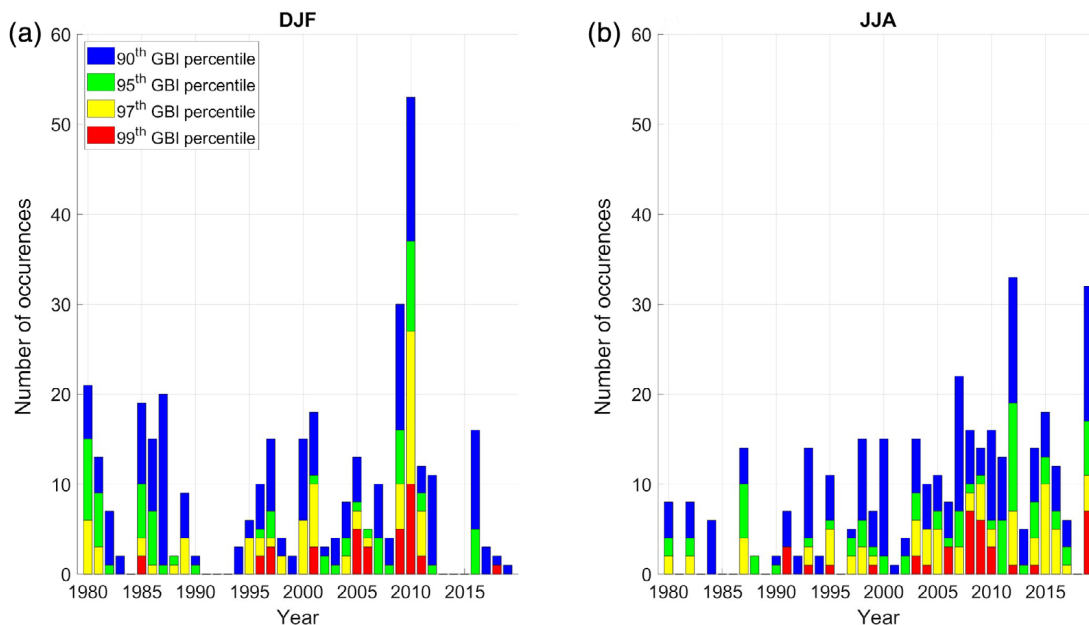


**FIGURE 2** Frequency of extreme Greenland Blocking Index (GBI) days per year from 1980 to 2019 in (a) DJF and (b) JJA, at the 90th, 95th, 97th, and 99th percentiles for each season

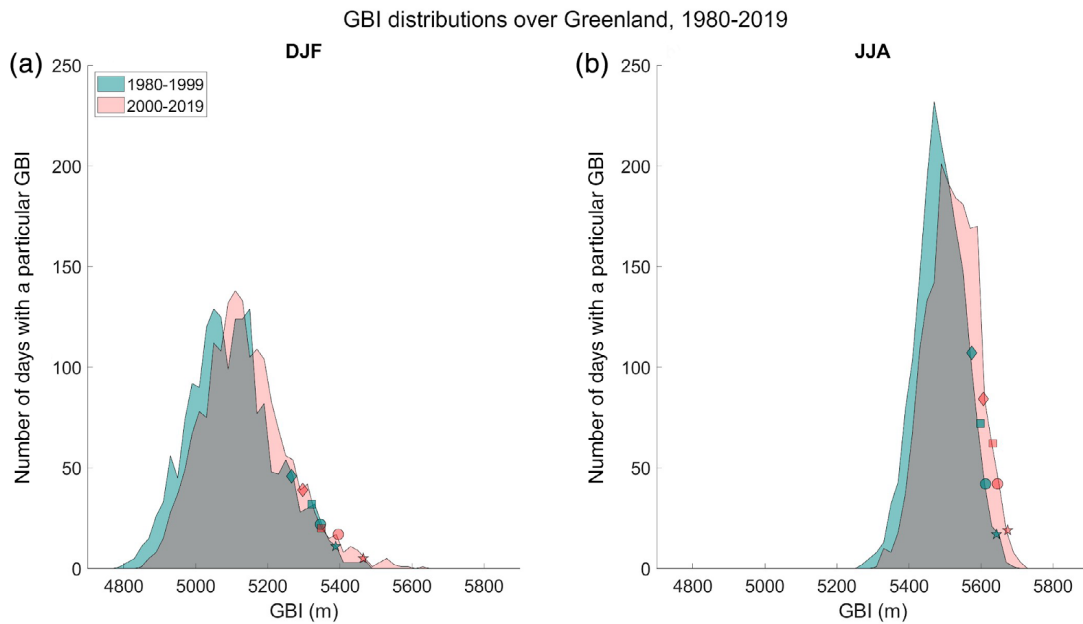


**FIGURE 3** Distributions of the NOAA GBI index for all days in 1980–1999 (teal distribution) and 2000–2019 (pink distribution) for (a) DJF and (b) JJA. The diamond, square, circle, and star symbols in each plot indicate the extreme thresholds of the 90th, 95th, 97th, and 99th percentile values, respectively

2000 is not always reflected by a similar grouping of extreme low NAO events (Hanna *et al.*, 2015), suggesting changes in *extreme* GBI may be due to a unique, local response, in spite of the more general relationships between flow blocking and the NAO (Woollings *et al.*, 2008; Rennert and Wallace, 2009; Hanna *et al.*, 2014).

Atmospheric flow blocking is a fundamental part of the circulation around and over Greenland. Extreme flow blocking over Greenland has been connected to ice mass balance changes, both for sea ice (Ballinger *et al.*, 2018) and the Greenland ice sheet (Hanna *et al.* 2013; McLeod and Mote, 2016). Moreover, advection of moisture can be consequential for mass balance changes in the Greenland ice sheet (McLeod and Mote, 2015; Mattingly *et al.*, 2016; 2018). Thus, it is important to explore the relationships between extreme flow blocking and moisture transport in and around Greenland, and that is the focus of the following section.

### 3.2 | Greenland blocking and moisture transport

Of the 358 winter days of extreme GBI at the 90th percentile, 78.4% of them were associated with above-normal IVT (values greater than the long-term mean) around Greenland (Table 2). The percentage of days with above-normal IVT increases especially for the more extreme GBI days: 88.3% of winter days with GBI above the 95th percentile featured above-normal IVT (Table 2), and

91.6% and 88.9% of winter days with GBI above the 97th and 99th percentiles, respectively, had above-normal IVT. In summer, the same pattern holds: days with extreme GBI featured above-normal IVT. For example, 63.3% of summer days with GBI above the 90th percentile had above-normal IVT, and the percentage increased to 75.7% for the 99th GBI percentile. Thus, in both summer and winter, high GBI tended to be accompanied by high IVT.

Extreme moisture transport, particularly through features called atmospheric rivers, can result in ice melt and mass loss as melt energy is provided by turbulent heat fluxes, driven by enhanced barrier winds that are in turn generated by a strong synoptic pressure gradient combined with an enhanced local temperature contrast between cool near-ice air and anomalously warm surrounding air (Mattingly *et al.*, 2018; 2020). Furthermore, Greenland blocking, and in particular *extreme* Greenland blocking, has increased in frequency and magnitude between 1980–1999 and 2000–2019 (Table 1 and Figure 2). It is thus important to examine the GBI–IVT relationship in greater depth. One way to do that is to repeat the above analysis, but for extreme IVT days, and examine the frequency of above-normal GBI during extreme IVT days. In winter, 63.4% of the days with IVT above the 90th percentile was associated with above-normal GBI (Table 2). That frequency of above-average GBI increased to 82.9% for the most extreme winter IVT (e.g., IVT at the 99th percentile). In summer, however, the relationship was mixed: between 45% and 50% of days

characterized by extreme IVT (above the 90th percentile) featured above-normal GBI. Thus, while high GBI is strongly associated with high IVT in both winter and summer, the reverse is mixed: wintertime extreme IVT days do tend to occur when the GBI is above normal, but summertime extreme IVT days do not necessarily occur when the GBI is above normal.

To further explore the GBI–IVT relationship, time leads and lags are examined. Because high IVT tended to occur on days with extreme GBI, the time leads and lags

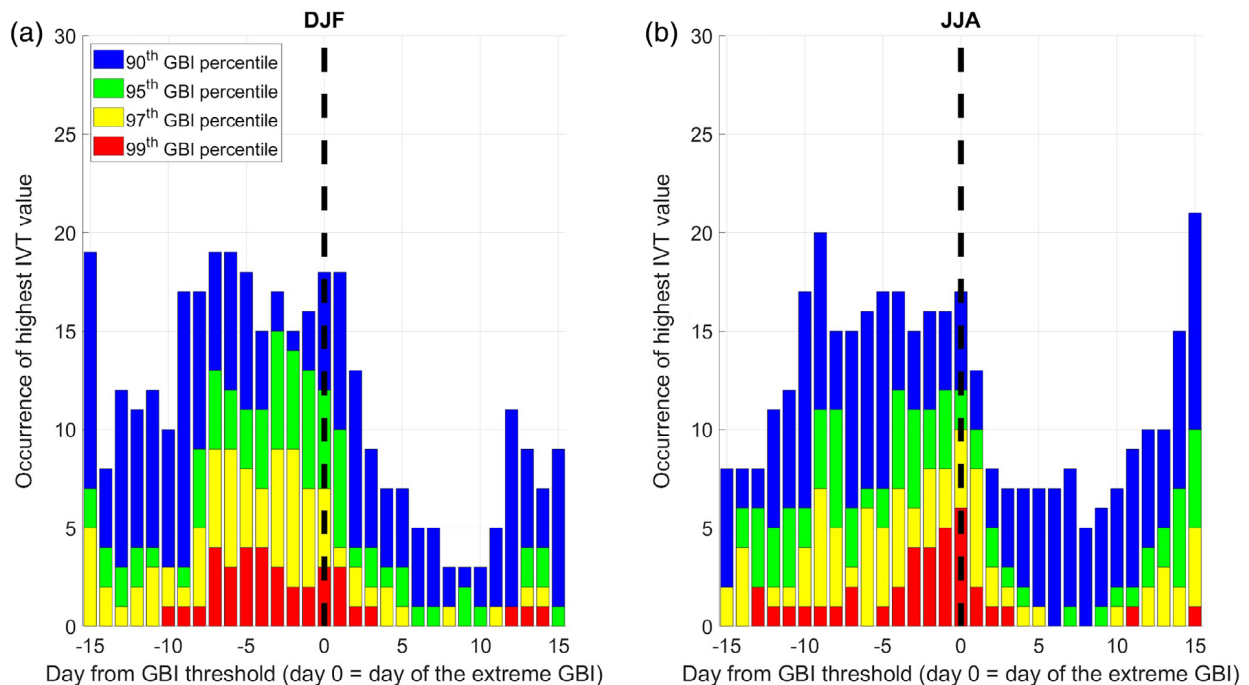
are defined with respect to the day of the extreme GBI. In winter, the highest IVT in the 30-day period centered on the date of the extreme GBI most often occurred from days –10 to +3 (10 days before the extreme GBI to 3 days after it) (Figure 4a). That pattern held for all four thresholds of winter GBI extremity: 90th, 95th, 97th, and 99th percentiles. Indeed, in winter, the highest IVT value occurred *on or before* the day of the extreme GBI between 68% and 83% of the time, with the highest IVT value occurring 77% of the time in the 15 days prior to the most

**TABLE 2** Seasonal likelihood of above average IVT days within varying extreme GBI thresholds (top). Seasonal likelihood of above average GBI days within varying extreme IVT thresholds (bottom)

GBI percentile	DJF			JJA		
	Days with high IVT	Total days	Percent (%)	Days with high IVT	Total days	Percent (%)
90th	281	358	78.5%	233	368	63.3%
95th	158	179	88.3%	136	184	73.9%
97th	98	107	91.6%	80	110	72.7%
99th	32	36	88.9%	28	37	75.7%

IVT percentile	DJF			JJA		
	Days with high GBI	Total days	Percent (%)	Days with high GBI	Total days	Percent (%)
90th	225	355	63.4%	170	368	46.2%
95th	119	177	67.2%	88	184	47.8%
97th	73	106	68.9%	54	110	49.1%
99th	29	35	82.9%	17	37	46.0%



**FIGURE 4** Frequency of above-average integrated vapor transport (IVT) indicating moisture transport for 15 days before to 15 days after an extreme blocking event in (a) DJF and (b) JJA. Black dashed line indicates the day of extreme blocking, and colors indicate extremity of the blocking event (from 90th to 99th percentile)

extreme GBI (99th) percentile (Figure 4a). This pattern held in summer, too: the highest IVT tended to occur on or before the date of extreme GBI (Figure 4b). Specifically, the highest IVT in the 31-day period centered on a day of extreme summer GBI occurred *on or before* the day of the extreme GBI between 62% (for the 90th percentile) and 84% (for the 99th percentile) of the days. On average the IVT peak occurs 2.5–3.6 days before an occurrence of extreme GBI in winter, while in summer, the IVT peak occurs 0.8–2.5 days before the extreme GBI, with the greatest lag occurring for the most extreme GBI (99th) percentile. This result means that extreme GBI events are very likely to be preceded by a peak in IVT, in both summer and winter, by several days.

## 4 | CONCLUSIONS

The overall goal of this study was to develop an understanding of the variability of *extreme* Greenland blocking from 1980 to 2019 and explore how moisture transport over Greenland varies with *extreme* Greenland blocking. Extreme blocking over Greenland was found to have increased in the most recent two decades (2000–2019) when compared to the two decades prior (1980–1999). This increase in extreme blocking agrees with others who have also studied blocking in and around Greenland (Fettweis *et al.*, 2013; Hanna *et al.*, 2015; 2018). Moreover, blocking was found to exhibit some interannual variability, in agreement with McLeod and Mote (2016), whereby years with frequent extreme blocking and years with scarce extreme blocking tending to cluster together. It is important to note that there may be a relationship between geopotential height over Greenland and other leading modes of atmospheric variability, both on shorter time scales (the NAO; Hanna *et al.*, 2015) and longer ones (the PDO; Collow *et al.*, 2017). In this study, we did not consider covariability between the GBI and those leading modes and suggest future work on that topic.

In addition, the probability of above-average IVT occurring on a day with extreme blocking is high in both summer and winter, with the highest probability of above-average IVT during an extreme GBI day in winter. The reverse relationship was more complex, with above-average blocking likely to occur during extreme winter IVT but not extreme summer IVT. This agrees with two related studies by Rimbu *et al.* (2007; 2008), who showed that during high blocking frequency over Greenland the axis of maximum moisture transport extends northward to Greenland relative to the times of low blocking frequency, leading to a more active storm track and greater moisture transport to the ice sheet. Finally, the highest

values of IVT were found to occur in advance of extreme GBI, tending to lead extreme GBI by between up to 2.5 days (in summer) and 3.6 days (in winter). These findings are unique to this work and lead to questions about the role of moisture transport in developing or sustaining blocks over Greenland, related to questions posed by McLeod and Mote (2015) on the role of precursor cyclones.

## ACKNOWLEDGEMENTS

Funding for this research was provided by award RC18-1658 from the Strategic Environmental Research and Development Program (SERDP). The authors wish to thank the three anonymous reviewers who provided helpful feedback to improve the manuscript.

## ORCID

Bradford S. Barrett  <https://orcid.org/0000-0002-5575-9052>

Gina R. Henderson  <https://orcid.org/0000-0001-6835-5658>

Thomas Mote  <https://orcid.org/0000-0002-0021-0134>

## REFERENCES

- Ballinger, T., Hanna, E., Hall, R., Cropper, T., Miller, J., Ribergaard, M., Overland, J.E. and Hoyer, J. (2018) Anomalous blocking over Greenland preceded the 2013 extreme early melt of local sea ice. *Annals of Glaciology*, 59, 181–190. <https://doi.org/10.1017/aog.2017.30>.
- Black, E., Blackburn, M., Harrison, G., Hoskins, B.J. and Methven, J. (2004) Factors contributing to the summer 2003 European heatwave. *Weather*, 59, 217–223. <https://doi.org/10.1256/wea.74.04>.
- Cheng, X. and Wallace, J.M. (1993) Cluster analysis of the northern hemisphere wintertime 500-hPa field: spatial patterns. *Journal of the Atmospheric Sciences*, 50, 2674–2696. <https://doi.org/10.1175/1520-0469.1175/1520-0469>.
- Collow, A., Mahanama, S.P., Bosilovich, M.G., Koster, R.D. and Schubert, S.D. (2017) An evaluation of teleconnections over the United States in an ensemble of AMIP simulations with the MERRA-2 configuration of the GEOS atmospheric model. *NASA/TM-2017-104606*, 47, 78. <https://gmao.gsfc.nasa.gov/pubs/docs/Collow963.pdf>.
- Croci-Maspoli, M., Schwierz, C. and Davies, H.C. (2007) A multifaceted climatology of atmospheric blocking and its recent linear trend. *Journal of Climate*, 20, 633–649.
- Davini, P., Cagnazzo, C., Gualdi, S. and Navarra, A. (2012) Bidimensional diagnostics, variability, and trends of northern hemisphere blocking. *Journal of Climate*, 25, 6496–6509. <https://doi.org/10.1175/JCLI-D-12-00032.1>.
- Davini, P., Cagnazzo, C., Fogli, P.G., Manzini, E., Gualdi, S. and Navarra, A. (2013) European blocking and Atlantic jet stream variability in the NCEP/NCAR reanalysis and the CMCC-CMS climate model. *Climate Dynamics*, 43, 71–85. <https://doi.org/10.1007/s00382-013-1873-y>.

- Dee, D.P., Uppala, S.M., Simmons, A.J., Berrisford, P., Poli, P., Kobayashi, S., Andrae, U., Balmaseda, M.A., Balsamo, G., Bauer, P., Bechtold, P., Beljaars, A.C.M., van de Berg, L., Bidlot, J., Bormann, N., Delsol, C., Dragani, R., Fuentes, M., Geer, A.J., Haimberger, L., Healy, S.B., Hersbach, H., Hólm, E. V., Isaksen, I., Kållberg, P., Köhler, M., Matricardi, M., McNally, A.P., Monge-Sanz, B.M., Morcrette, J.J., Park, B.K., Peubey, C., de Rosnay, P., Tavolato, C., Thépaut, J.N. and Vitart, F. (2011) The ERA-interim reanalysis: configuration and performance of the data assimilation system. *Quarterly Journal of the Royal Meteorological Society*, 137(656), 553–597. <https://doi.org/10.1002/qj.828>.
- Ding, Q., Wallace, J.M., Battisti, D.S., Steig, E.J., Gallant, A.J., Kim, H.J. and Geng, L. (2014) Tropical forcing of the recent rapid Arctic warming in northeastern Canada and Greenland. *Nature*, 509(7499), 209–212.
- Dole, R.M. and Gordon, N.D. (1983) Persistent anomalies of the extratropical northern hemisphere wintertime circulation: geographical distribution and regional persistence characteristics. *Monthly Weather Review*, 111, 1567–1586. <https://doi.org/10.1175/1520-0493>.
- Dole, R.M. (1986) Persistent anomalies of the extratropical northern hemisphere wintertime circulation: structure. *Monthly Weather Review*, 114, 178–207. <https://doi.org/10.1175/1520-0493>.
- Dole, R., Hoerling, M., Perlwitz, J., Eischeid, J., Pegion, P., Zhang, T., Quan, X.-W., Xu, T. and Murray, D. (2011) Was there a basis for anticipating the 2010 Russian heat wave? *Geophysical Research Letters*, 38, L06702. <https://doi.org/10.1029/2010GL046582>.
- Dufour, A., Zolina, O. and Gulev, S.K. (2016) Atmospheric moisture transport to the Arctic: assessment of reanalyses and analysis of transport components. *Journal of Climate*, 29, 5061–5081. <https://doi.org/10.1175/JCLI-D-15-0559.1>.
- Fang, Z.-F. (2004) Statistical relationship between the northern hemisphere sea ice and atmospheric circulation during winter time. In: Zhu, X. (Ed.) *Observation, Theory and Modeling of Atmospheric Variability. World Scientific Series on Meteorology of East Asia*. Singapore: World Scientific Publishing Company, pp. 131–141.
- Fettweis, X., Hanna, E., Lang, C., Belleflamme, A., Ericum, M. and Gallée, H. (2013) Important role of the mid-tropospheric atmospheric circulation in the recent surface melt increase over the Greenland ice sheet. *The Cryosphere*, 7, 241–248. <https://doi.org/10.5194/tc-7-241-2013>.
- Francis, J.A. and Vavrus, S.J. (2015) Evidence for a wavier jet stream in response to rapid Arctic warming. *Environmental Research Letters*, 10, 014005. <https://doi.org/10.1088/1748-9326/10/1/014005>.
- Gimeno, L., Nieto, R., Vázquez, M. and Lavers, D.A. (2014) Atmospheric rivers: a mini-review. *Frontiers in Earth Science*, 2, 2. <https://doi.org/10.3389/feart.2014.00002>.
- Gimeno-Sotelo, L., Nieto, R., Vázquez, M. and Gimeno, L. (2018) A new pattern of the moisture transport for precipitation related to the Arctic Sea ice extent drastic decline. *Earth System Dynamics*, 9, 611–625. <https://doi.org/10.5194/esd-9-611-2018>.
- Hanna, E., Jones, J.M., Cappelen, J., Mernild, S.H., Wood, L., Steffen, K. and Huybrechts, P. (2013) The influence of North Atlantic atmospheric and oceanic forcing effects on 1900–2010 Greenland summer climate and ice melt/runoff. *International Journal of Climatology*, 33, 862–880. <https://doi.org/10.1002/joc.3475>.
- Hanna, E., Fettweis, X., Mernild, S.H., Cappelen, J., Ribergaard, M. H., Shuman, C.A., Steffen, K., Wood, L. and Mote, T.L. (2014) Atmospheric and oceanic climate forcing of the exceptional Greenland ice sheet surface melt in summer 2012. *International Journal of Climatology*, 34, 1022–1037. <https://doi.org/10.1002/joc.3743>.
- Hanna, E., Cropper, T.E., Jones, P.D., Scaife, A.A. and Allan, R. (2015) Recent seasonal asymmetric changes in the NAO (a marked summer decline and increased winter variability) and associated changes in the AO and Greenland blocking index. *International Journal of Climatology*, 35, 2540–2554. <https://doi.org/10.1002/joc.4157>.
- Hanna, E., Hall, R.J., Cropper, T.E., Ballinger, T.J., Wake, L., Mote, T. and Cappelen, J. (2018) Greenland blocking index daily series 1851–2015: analysis of changes in extremes and links with North Atlantic and UK climate variability and change. *International Journal of Climatology*, 38(9), 3546–3564. <https://doi.org/10.1002/joc.5516>.
- Hartmann, D., et al. (2013) Observations: atmosphere and surface. In: Stocker, T.F., et al. (Eds.) *Climate Change 2013: The Physical Science Basis*. Cambridge: Cambridge University Press, pp. 159–254.
- Held, I.M. and Soden, B.J. (2006) Robust responses of the hydrological cycle to global warming. *Journal of Climate*, 19(21), 5686–5699.
- Hoskins, B.J. and Sardeshmukh, P.D. (1987) A diagnostic study of the dynamics of the northern hemisphere winter of 1985–1986. *Quarterly Journal of the Royal Meteorological Society*, 113, 759–778. <https://doi.org/10.1002/qj.49711347705>.
- Hurrell, J.W., Kushnir, Y., Ottersen, G. and Visbeck, M. (2003) The North Atlantic Oscillation. Climatic significance and environmental impact. In: *Geophysical Monograph*, Vol. 134. Washington, DC: American Geophysical Union.
- Langford, E. (2006) Quartiles in elementary statistics. *Journal of Statistical Education*, 14, 3. <https://doi.org/10.1080/10691898.2006.11910589>.
- Lavers, D.A., Ralph, F.M., Waliser, D.E., Gershunov, A. and Dettinger, M.D. (2015) Climate change intensification of horizontal water vapor transport in CMIP5. *Geophysical Research Letters*, 42, 5617–5625. <https://doi.org/10.1002/2015GL064672>.
- Legras, B. and Ghil, M. (1985) Persistent anomalies, blocking and variations in atmospheric predictability. *Journal of the Atmospheric Sciences*, 42, 433–471. <https://doi.org/10.1175/1520-0469>.
- Lejenas, H. and Okland, H. (1983) Characteristics of northern hemisphere blocking as determined from a long time series of observational data. *Tellus*, 35A, 360–362. <https://doi.org/10.1111/j.1600-0870.1983.tb00210.x>.
- Li, Z., Zhang, W., Stuecker, M.F., Xu, H., Jin, F.F. and Liu, C. (2019) Different effects of two ENSO types on Arctic surface temperature in boreal winter. *Journal of Climate*, 32(16), 4943–4961.
- Liu, C. and Barnes, E.A. (2015) Extreme moisture transport into the Arctic linked to Rossby wave breaking. *Journal of Geophysical Research: Atmospheres*, 120(9), 3774–3788.
- Mantua, N.J., Hare, S.R., Zhang, Y., Wallace, J.M. and Francis, R.C. (1997) A Pacific interdecadal climate oscillation with impacts

- on salmon production. *Bulletin of the American Meteorological Society*, 78, 1069–1079.
- Marsaglia, G., Tsang, W. and Wang, J. (2003) Evaluating Kolmogorov's distribution. *Journal of Statistical Software*, 8(18), 1–4. <https://doi.org/10.18637/jss.v008.i18>.
- Masato, G., Hoskins, B.J. and Woollings, T.J. (2012) Wave-breaking characteristics of midlatitude blocking. *Quarterly Journal of the Royal Meteorological Society*, 138(666), 1285–1296.
- Massey, F.J. (1951) The Kolmogorov–Smirnov test for goodness of fit. *Journal of the American Statistical Association*, 46(253), 68–78.
- Mattingly, K.S., Ramseyer, C.A., Rosen, J.J., Mote, T.L. and Muthyala, R. (2016) Increasing water vapor transport to the Greenland ice sheet revealed using self-organizing maps. *Geophysical Research Letters*, 43, 9250–9258. <https://doi.org/10.1002/2016GL070424>.
- Mattingly, K.S., Mote, T.L. and Fettweis, X. (2018) Atmospheric river impacts on Greenland ice sheet surface mass balance. *Journal of Geophysical Research: Atmospheres*, 123, 8538–8560. <https://doi.org/10.1029/2018JD028714>.
- Mattingly, K.S., Mote, T.L., Fettweis, X., van As, D., Van Tricht, D., Lhermitte, S. and Pettersen, C. (2020) Strong summer atmospheric rivers trigger Greenland ice sheet melt through spatially varying surface energy balance and cloud regimes. *Journal of Climate*. <https://doi.org/10.1175/JCLI-D-19-0835.1>.
- McLeod, J.T. and Mote, T.L. (2016) Linking interannual variability in extreme Greenland blocking episodes to the recent increase in summer melting across the Greenland ice sheet. *International Journal of Climatology*, 36, 1484–1499. <https://doi.org/10.1002/joc.4440>.
- McLeod, J.T. and Mote, T.L. (2015) Assessing the role of precursor cyclones on the formation of extreme Greenland blocking episodes and their impact on summer melting across the Greenland ice sheet. *Journal of Geophysical Research Atmospheres*, 120, 12357–12377. <https://doi.org/10.1002/2015JD023945>.
- Michelangeli, P.A., Vauturd, A. and Legras, B. (1995) Weather regimes: recurrence and quasi-stationarity. *Journal of the Atmospheric Sciences*, 52, 1237–1256. <https://doi.org/10.1175/1520-0469>.
- Miller, L.H. (1956) Table of percentage points of Kolmogorov statistics. *Journal of the American Statistical Association*, 51(273), 111–121.
- Namias, J. (1982) *Short period climatic variations-Collected works of J. Namias: Volumes I and II (1934 through 1974), Volume III (1975 through 1982)*. University of California San Diego Press, San Diego, CA, 393 p.
- Nusbaumer, J., Alexander, P.M., LeGrande, A.N. and Tedesco, M. (2019) Spatial shift of Greenland moisture sources related to enhanced Arctic warming. *Geophysical Research Letters*, 46(24), 14723–14731. <https://doi.org/10.1029/2019GL084633>.
- Nygård, T., Graverson, R.G., Uotila, P., Naakka, T. and Vihma, T. (2019) Strong dependence of wintertime Arctic moisture and cloud distributions on atmospheric large-scale circulation. *Journal of Climate*, 32(24), 8771–8790.
- Osborn, T.J. (2011) Winter 2009/2010 temperatures and a record-breaking North Atlantic Oscillation index. *Weather*, 66, 19–21. <https://doi.org/10.1002/wea.660>.
- Overland, J.E., Francis, J.A., Hall, R., Hanna, E., Kim, S.-J. and Vihma, T. (2015) The melting Arctic and mid-latitude weather patterns: are they connected? *Journal of Climate*, 28, 7917–7932. <https://doi.org/10.1175/JCLI-D-14-00822.1>.
- Pelly, J. and Hoskins, B.J. (2003) A new perspective on blocking. *Journal of the Atmospheric Sciences*, 60, 743–755. <https://doi.org/10.1175/1520-0469>.
- Polyakov, I.V., Alekseev, G.V., Bekryaev, R.V., Bhatt, U., Colony, R. L., Johnson, M.A., Karklin, V.P., Makshtas, A.P., Walsh, D. and Yulin, A.V. (2002) Observationally based assessment of polar amplification of global warming. *Geophysical Research Letters*, 29, 1878. <https://doi.org/10.1029/2001GL011111>.
- Rasmussen, E.M. and Wallace, J.M. (1983) Meteorological aspects of the El Niño/southern oscillation. *Science*, 222, 119–1202.
- Rennert, K.J. and Wallace, J.M. (2009) Cross-frequency coupling, skewness, and blocking in the northern hemisphere winter circulation. *Journal of Climate*, 22, 5650–5666.
- Rex, D.F. (1950a) Blocking action in the middle troposphere and its effect on regional climate. Part I: an aerological study of blocking action. *Tellus*, 2, 196–211. <https://doi.org/10.1111/j.2153-3490.1950.tb00331.x>.
- Rex, D.F. (1950b) Part II: the climatology of blocking action. *Tellus*, 2, 275–301.
- Rimbu, N., Lohmann, G. and Grosfeld, K. (2007) Northern hemisphere atmospheric blocking in ice core accumulation records from northern Greenland. *Geophysical Research Letters*, 34, L09704.
- Rimbu, N., Lohmann, G. and Grosfeld, K. (2008) Northern hemisphere atmospheric blocking in ice core accumulation records from northern Greenland. *PAGES News*, 16, 5–7.
- Rinke, A., Segger, B., Crewell, S., Maturilli, M., Naakka, T., Nygård, T., Vihma, T., Alshawaf, F., Dick, G. and Wickert, J. (2019) Trends of vertically integrated water vapor over the Arctic during 1979–2016: consistent moistening all over? *Journal of Climate*, 32, 6097–6116.
- Rutz, J.J., Steenburgh, W.J. and Ralph, F.M. (2014) Climatological characteristics of atmospheric rivers and their inland penetration over the western United States. *Monthly Weather Review*, 142(2), 905–921. <https://doi.org/10.1175/MWR-D-13-00168.1>.
- Scherrer, S.C., Croci-Maspoli, M., Schwierz, C. and Appenzeller, C. (2006) Two-dimensional indices of atmospheric blocking and their statistical relationship with winter climate patterns in the euro-Atlantic region. *International Journal of Climatology*, 26, 233–249. <https://doi.org/10.1002/joc.1250>.
- Screen, J.A. and Simmonds, I. (2010) The central role of diminishing sea ice in recent arctic temperature amplification. *Nature*, 464, 1334–1337. <https://doi.org/10.1038/nature09051>.
- Serreze, M.C., Barrett, A., Stroeve, J., Kindig, D. and Holland, M. (2009) The emergence of surface-based arctic amplification. *The Cryosphere*, 3, 11–19. <https://doi.org/10.5194/tc-3-11-2009>.
- Sorteberg, A. and Walsh, J.E. (2008) Seasonal cyclone variability at 70°N and its impact on moisture transport into the Arctic. *Tellus A: Dynamic Meteorology and Oceanography*, 60(3), 570–586. <https://doi.org/10.1111/j.1600-0870.2007.00314.x>.
- Smyth, P., Idle, K. and Ghil, M. (1999) Multiple regimes in northern hemisphere height fields via mixture model clustering. *Journal of the Atmospheric Sciences*, 56, 3704–3723. <https://doi.org/10.1175/1520-0469>.
- Tibaldi, T. and Molteni, F. (1990) On the operational predictability of blocking. *Tellus*, 42A, 343–365. <https://doi.org/10.1034/j.1600-0870.1990.t01-2-00003.x>.

- Tyrlis, E. and Hoskins, B.J. (2008) Aspects of a northern hemisphere atmospheric blocking climatology. *Journal of the Atmospheric Sciences*, 65, 1638–1652. <https://doi.org/10.1175/2007JAS2337.1>.
- Vautard, R. (1990) Multiple weather regimes over the North Atlantic: analysis of precursors and successors. *Monthly Weather Review*, 118, 2056–2081. <https://doi.org/10.1175/1520-0493>.
- Woods, C., Caballero, R. and Svensson, G. (2013) Large-scale circulation associated with moisture intrusions into the Arctic during winter. *Geophysical Research Letters*, 40, 4717–4721. <https://doi.org/10.1002/grl.50912>.
- Woollings, T., Hoskins, B., Blackburn, M. and Berrisford, P. (2008) A new Rossby wave–breaking interpretation of the North Atlantic oscillation. *Journal of the Atmospheric Sciences*, 65(2), 609–626.
- Yang, W. and Magnusdottir, G. (2017) Springtime extreme moisture transport into the Arctic and its impact on sea ice concentration. *Journal of Geophysical Research Atmosphere*, 122, 5316–5329. <https://doi.org/10.1002/2016JD026324>.

**How to cite this article:** Barrett BS, Henderson GR, McDonnell E, Henry M, Mote T. Extreme Greenland blocking and high-latitude moisture transport. *Atmos Sci Lett*. 2020;e1002. <https://doi.org/10.1002/asl.1002>